cAMP Modulation of the Cytoplasmic Domain in the HCN2 Channel Investigated by Molecular Simulations

Marco Berrera,* Sergio Pantano,*† and Paolo Carloni*
*Scuola Internazionale Superiore di Studi Avanzati and Istituto Nazionale per la Fisica della Materia, Democritos Modeling Center for Research in Atomic Simulation, Trieste, Italy; and †Venetian Institute of Molecular Medicine, Padova, Italy

ABSTRACT The hyperpolarization-activated cyclic nucleotide-modulated (HCN) cation channels are opened by membrane hyperpolarization, while their activation is modulated by the binding of cyclic adenosine monophosphate (cAMP) in the cytoplasm. Here we investigate the molecular basis of cAMP channel modulation by performing molecular dynamics simulations of a segment comprising the C-linker and the cyclic nucleotide binding domain (CNBD) in the presence and absence of cAMP, based on the available crystal structure of HCN2 from mouse. In presence of cAMP, the protein undergoes an oscillation of the quaternary structure on the order of 10 ns, not observed in the apoprotein. In contrast, the absence of ligand causes conformational rearrangements within the CNBDs, driving these domains to a more flexible state, similar to that described in CNBDs of other proteins. This increased flexibility causes a rather disordered movement of the CNBDs, resulting in an inhibitory effect on the channel. We propose that the cAMP-triggered large-scale oscillation plays an important role for the channel's function, being coupled to a motion of the C-linker which, in turn, modulates the gating of the channel.

INTRODUCTION

The hyperpolarization-activated cyclic nucleotide-modulated (HCN) cation channels family includes, in vertebrates, four members (HCN1–4) involved in cardiac and neuronal pacemaker activity. These channels, which belong to the voltage-gated channels superfamily, are opened by membrane hyperpolarization, while the binding of cyclic adenosine monophosphate (cAMP) modulates their activity (1–16).

HCN channels are tetrameric and each monomer comprises three conserved domains. The transmembrane domain, which is responsible for the ion selectivity and gating, is connected to the C-linker domain in the cytoplasm, which in turn is linked to the cyclic nucleotide binding domain (CNBD).

HCN2 is the most characterized member of the family. In this channel, CNBD inhibits channel activity by a mechanism that depends on the C-linker/CNBD interactions: binding of cAMP relieves this inhibition and shifts the voltage dependence by $\sim+17$ mV to less negative values (15,16). In a seminal article (17), Zagotta and co-workers have determined the x-ray structure of C-linker and CNBD of HCN2 from mouse in complex with four equivalents of cAMP (Fig. 1, *a* and *b*). The C-linker is composed by six α-helices (A′–F′), establishing a large amount of intersubunit contacts and coupling the ion-channel gating transmembrane part to the CNBD (17,18). The CNBD includes four α-helices (A, P, B, C) and an eight-stranded β-roll, arranged with the same fold of other CNBDs (19–27). cAMP binds in its *anti*-conformation to a highly conserved region lined by the β-rolls, P-, and C-helices (Fig. 1, *a* and *d*). Its phosphate and OH groups H-bond to a group of residues from 581 to 593, which includes the P-helix and the following loop. These residues constitute the signature motif of the CNBDs, called the phosphate-binding cassette (28). The purinic group of the ligand forms contacts with β-strands 4 and 5 (Val-564, Met-572, and Leu-574) and the C-helix (Arg-632 and Ile-636) (17).

Recently, molecular dynamics (MD) simulations provided valuable insights in the regulation mechanisms in different ionic channels (such as the nicotinic receptor and the Kir channel) under conditions that are difficult to achieve with experimental techniques (29–33). Based on the available structural information (17), here we study the cytoplasmic part of HCN2 by means of MD simulations, to provide a description of the molecular process driven by cAMP leading to channel modulation. Based on our calculations, we propose that the allosteric mechanism of cAMP modulation originates from oscillations of CNBD quaternary structure around its average structure, with a periodicity in the order of 10 ns. This large-scale breathing motion is triggered by cAMP binding: in fact, in the absence of the ligand, CNBD assumes a rather disordered and loose structure, similarly to what has been found in other CNBDs with the same fold (20,23,28,34,35) and no quaternary structure oscillations are observed.

COMPUTATIONAL METHODS

The holoprotein is the x-ray structure of the cytoplasmic domains of HCN2 channel from mouse in complex with four equivalents of cAMP, solved at 2.30 Å resolution (residues 443–645, PDB entry No. 1Q5O (17,36)). The protein is a homotetramer, with a fourfold rotational symmetry (Fig. 1, *a* and *b*). The apoprotein is obtained by removing the four cAMPs. Hydrogen atoms are added by assuming standard bond lengths and bond angles. Histidines 463, 474, 479, and 559 are protonated respectively on their Nϵ, Nδ, Nϵ, and Nδ, as this choice optimizes the formation of the H-bond network with their surroundings. Acid and basic residues are assumed to be

Submitted July 29, 2005, and accepted for publication January 25, 2006.

Address reprint requests to P. Carloni, Tel.: 39-040-378-7407; E-mail: carloni@sissa.it.

0006-3495/06/05/3428/06 $2.00

doi: 10.1529/biophysj.105.071621

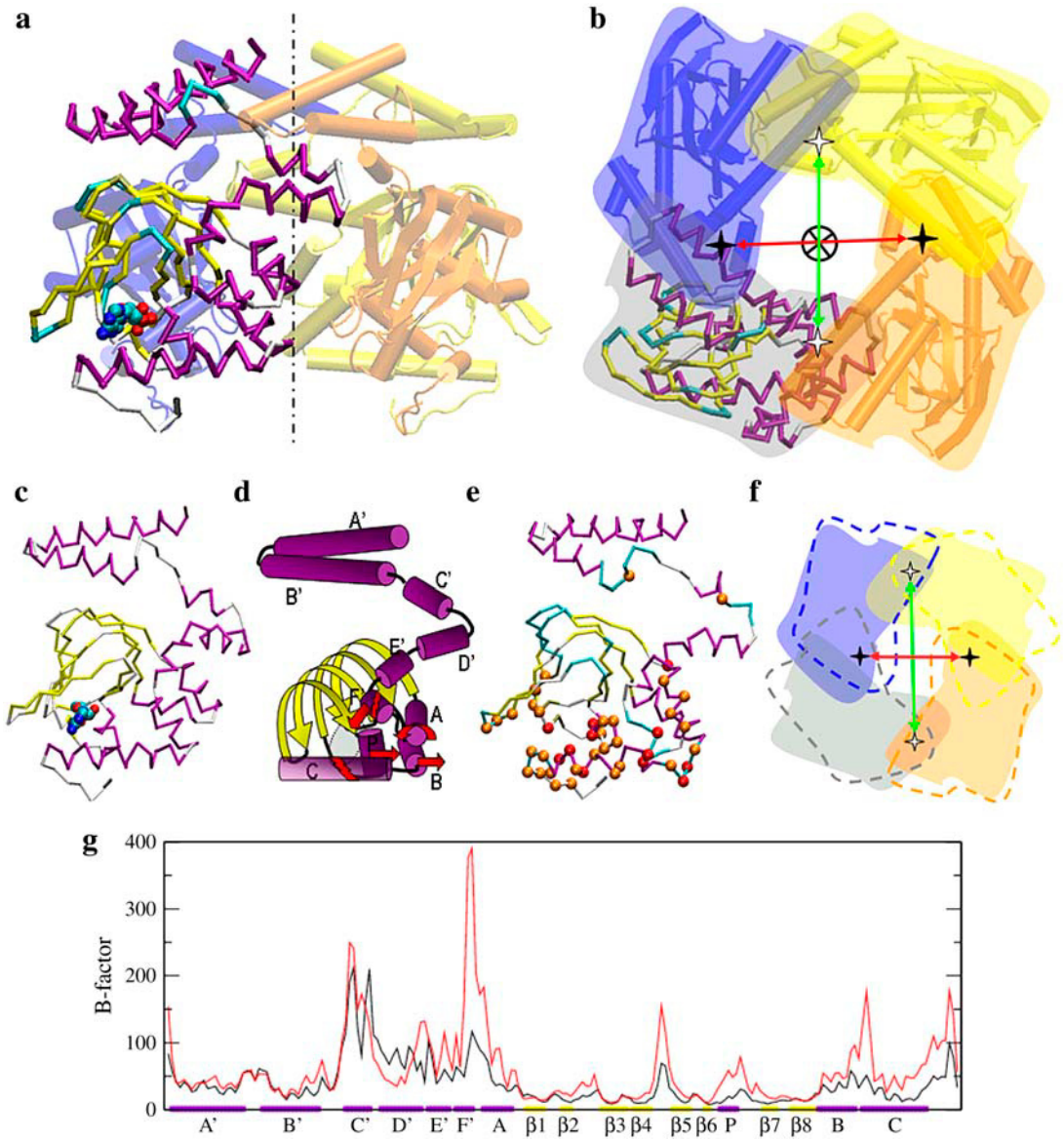

FIGURE 1 (*a*) Structure of C-linker and CNBD of HCN2 from mouse (17): four subunits are arranged around the fourfold rotational symmetry axis, which is represented by the dashed line, forming the homotetramer. C-linkers are at the top and CNBDs at the bottom of the picture. Three subunits are drawn in cartoons and in the fourth, which is drawn in trace, secondary structure elements are colored in violet for helices and yellow for β-strands and one cAMP molecule is shown. (*b*) Upper view of the complex: stars indicate mass centers of opposite couples of adjacent subunits. (*c*) Diagram of one subunit of HCN2 C-linker and CNBD with cAMP in its binding site. (*d*) Cascade of helices rearrangements after ligand unbinding (20,23,28,34). (*e*) Representative snapshot of the apoprotein, to be compared with *c*: balls represent residues whose B-factor in the apoprotein is at least two (*orange*) and three (*red*) times that in the holoprotein, which are spread in the CNBD and E′- and F′-helices, including residues forming the binding site. (*f*) The most relevant motions in the holoprotein are oscillations of the quaternary structure, which are here identified by the distances between mass centers of opposite couples of adjacent subunits (*stars* as in *b*) and are plotted in Fig. 2, *c* and *d*. (*g*) B-factors in the holoprotein (*black line*) and in the apoprotein (*red line*) are plotted along the sequence. Secondary structure elements are indicated in violet for helices and yellow for β-strands, and are labeled.

ionized at the physiological conditions. The models are immersed in parallelepiped boxes whose edges are ~10.0, 10.0, and 8.1 nm, containing ~22,500 water molecules; 12 and 16 chlorine ions are added to neutralize the boxes.

The AMBER99 (37–39) and the TIP3P (40) force fields are used for the protein (and ions) and water, respectively; parameters for cAMP are obtained from Punta et al. (41). Rectangular periodic boundary conditions are applied. Particle-mesh Ewald is used to evaluate long-range electrostatics (42–44). A cutoff of 1 nm is used for the real part of the electrostatics and van der Waals interactions. The neighbor list is updated every 10 steps. Constraints are applied to the chemical bonds using the LINCS algorithm (45). The integration time step is set to 1.5 fs.

The MD program GROMACS is used (46,47). After energy minimization, 45 ps of MD of the solvent and a gradual heating of the systems (eight runs, 22.5 ps each, from 0 to 10, 30, 70, 100, 150, 200, 250, 300 K, using the Berendsen thermostat and barostat (48)), the complexes undergo 2.3 ns of MD in the NPT ensemble at 300 K and 1 atm pressure, using the Nosé-Hoover thermostat (49,50) and the Parrinello-Rahman barostat (51,52); the

pressure coupling is isotropic in all directions. After ~2 ns, the average root mean-square deviation (RMSD) for single subunits fluctuates around 0.15 nm in both systems (Fig. 2, *a* and *b*). Finally, 19.7 ns MDs are performed in the NVT ensemble, using the Nosé-Hoover thermostat (49,50).

The following properties are calculated:

1. RMSDs are calculated with respect to the x-ray structure (46,47).
2. B-factors are calculated after fitting the four subunits to the starting conformation of one monomer (46,47).
3. Essential modes (EMs) are obtained diagonalizing the covariance matrix (46,47,53–57): cosine contents are calculated for the first 10 eigenvectors (46,47,58,59).
4. Intersubunit contact surface is evaluated as the difference between solvent-accessible surface areas (46,47,60,61) calculated for isolated subunits and for the tetramer.
5. The secondary structure elements are identified by the program DSSP (62).

Properties 1–3 are calculated considering only Cα and properties 2–4 are calculated for the last 20 ns of MD.

To complement the study of the protein dynamic properties, we perform elastic network analysis by applying a modified version of the Gaussian model, which consider also the Cβ atoms (63).

RESULTS

Holoprotein

During the MD simulation, the RMSD of the ligand-bound protein increases up to nearly 0.2 nm within the first 2 ns; subsequently, the RMSD fluctuates between 0.2 and 0.3 nm (Fig. 2 *a*), with an overall oscillation in the ~13-ns timescale. Also the distances between centers-of-mass of two complex halves (Fig. 1, *b* and *f*), which are perpendicular to the homotetramer rotational symmetry, oscillate with the same period and an amplitude of ~0.05 nm (Fig. 2 *c* and Fig. 1, *b* and *f*). The protein oscillates between a configuration similar to that of the x-ray structure and a conformation where two opposite intersubunit interface regions are more distant than the other two. The projection of the first EM on the real space trajectory reproduces this movement (see Fig. 1, Supplementary Material, and animation available at http://www.sissa.it/~berrera/HCN2/movies.html). The corresponding eigenvalue accounts for ~24% of the total fluctuations. No large intrasubunit rearrangements are observed and the RMSD of single subunit is nearly 0.15 nm (Fig. 2 *a*). The cosine contents of the first 10 EMs are as small as 0.2, indicating that the simulation is rather converged (58,59). A Gaussian elastic network model (63) calculation provides a similar picture: the two slowest normal modes describe conformational motions that evolve perpendicularly to the homotetramer axis (animation at the address above), similar to that obtained from the EM analysis of the MD trajectory. The scalar product of the first EM with the first and the second β-Gaussian normal modes are 0.5 each, and the subspace overlap of the first EM with the first 10 β-Gaussian normal modes is 0.82, meaning that the first EM is well described in the vibrations of the elastic network model. Moreover, the eigenvalues of the first 10 EMs, which account for ~70% of the total fluctuations, correlate with the corresponding eigenvalues of the β-Gaussian normal modes (see Fig. 2, Supplementary Material). In addition, the secondary structure elements and the protein/ligand contacts observed in the x-ray structure are fully maintained throughout the MD trajectory.

Apoprotein

Also, the RMSD of the ligand free protein increases up to nearly 0.2 nm within the first 2 ns, and subsequently fluctuates between 0.2 and 0.3 nm without the oscillation

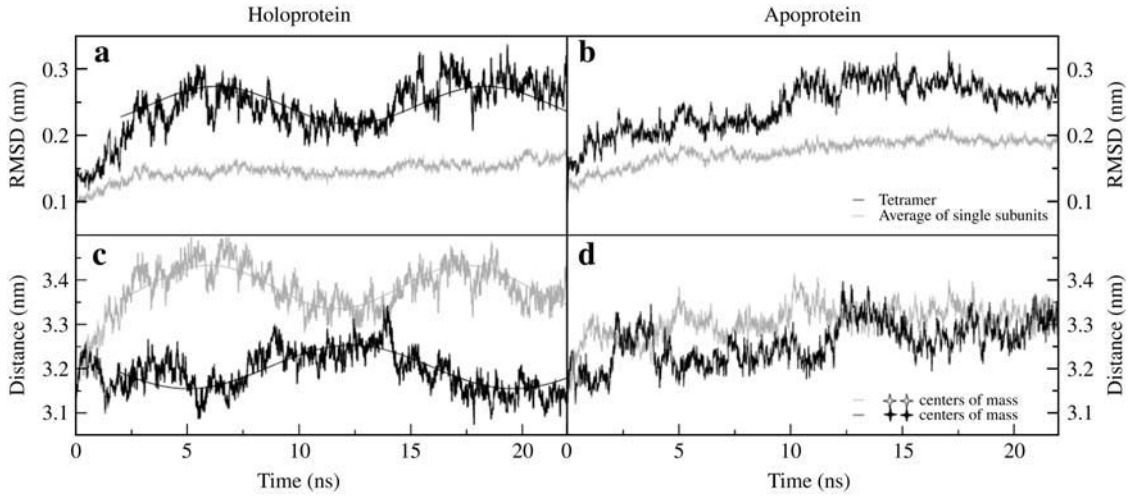

FIGURE 2 Cα RMSD plots (*a*,*b*) and distances between mass centers of opposite couples of adjacent subunits (*c*,*d*) according to Fig. 1, *b* and *f*, in the holoprotein (*a*,*c*) and in the apoprotein (*b*,*d*). RMSD for the tetramer (*solid*) and average RMSD for single chains (*shaded*) are shown. For the holoprotein, distances and RMSD plots are correlated and display an oscillation that can be fitted by a sine function with a period of ~13 ns and an amplitude of ~0.03 nm for RMSD and ~0.05 nm for both centers-of-mass distances.

identified above (Fig. 2 *b*). A plot of the distances between the same centers-of-mass defined above confirms that the quaternary structure does not oscillate as in the cAMP-bound system (Fig. 2 *d*). In addition, the motion of each subunit is uncorrelated to that of the others. The RMSDs of each subunit fluctuate at ~0.2 nm toward the end of the simulation (Fig. 2 *b*), suggesting that in this case fluctuations within single chains are more relevant. In fact, the absence of the ligand causes a cascade of dramatic rearrangements first affecting C- and P-helices, which are elements forming the binding pocket. These rearrangements have been already observed in CNBDs of other proteins with the same fold (20,23,28,34,35,41) and are here only briefly summarized (Fig. 1 *d*). The C-helix breaks, increasing the flexibility of its extremities. This allows for a rotation of the P-helix around its longitudinal axis as observed in other CNBDs (20,23,34). The movements of the C- and P-helices are also transferred to helices B, A, and F′, this last within the C-term part of the C-linker. F′-helix moves closer to C-helix of CNBD and its secondary structure breaks. These rearrangements are linked to residues bearing higher flexibility, as evidenced by a comparison of the B-factors in the apoprotein with those of the holoprotein (Fig. 1, *e* and *g*). The cosine content of the largest EM is 0.8 and those of the following nine are as small as 0.2, probably suggesting that the system has not yet reached a fully converged state.

Finally, the intersubunit interaction appears to be stronger in the apoprotein than in the holoprotein, because the intersubunit contact surface is respectively 74 (2) nm^2 and 69 (2) nm^2 (64), compatible with the fact that, in the holoprotein, the subunits undergo large oscillations, one relative to the other.

DISCUSSION AND CONCLUSION

Protein fluctuations play a crucial role for a large variety of protein functions (65,66). In this work, we have shown that MD simulations provide complementary and important information not emerging from the x-ray structure of the complex between the cytoplasmic domains of HCN2 and cAMP. In fact, the motion of the holoprotein is characterized by quaternary structure oscillation, hinged at the intersubunit contact surface: two opposite edges of the complex go far closer, with a period of ~13 ns (Fig. 1 *f*, Fig. 2 *c*, and animation at http://www.sissa.it/~berrera/HCN2/movies.html). Elastic network analysis supports these conclusions.

A reduction of the intersubunit interactions due to electrostatics has been proposed to facilitate the opening transition of the C-linker (67,68). Thus, at the speculative level, we also propose that the weakening of the van der Waals interactions can play a role for gating. In fact, our calculations indicate that the cAMP binding induces a reduction in the contact surfaces between subunits, i.e., it leads to a weakening of the intersubunit van der Waals interaction.

The MD simulations provide also insights on the cytoplasmic domains in the ligand-free form, for which no structural information is available. CNBD experiences a cascade of rearrangements of secondary structure elements: the repositioning of P-helix and the increased flexibility of C-helix lead to a reorientation of B-helix, which in turn affects A-helix and the C-terminal part of C-linker (Fig. 1 *d*). Very similar cascades of events have been seen previously in the context of CNBDs with the same fold in different proteins (34), pointing to a ligand-dependent orientation of C-helix relative to the β-roll (28,35,41) and to a conformational change in the phosphate-binding cassette after ligand release coupled to a reorientation of the B-helix by hydrophobic residues, which are conserved in CNBDs from different proteins and corresponds in HCN2 to Leu-585 of P-helix and Phe-611 of B-helix (20,23,28). In fact, in the apoprotein a rotation of the P-helix turns the Leu-585 side chain to push the Phe-611 side chain.

In conclusion, MD simulations allow us to dissect important aspects of the mechanism for cAMP allosteric modulation in the HCN2 channel. We must note that the structural features reported here for the cAMP free and bound systems are confined to the relatively short timescale allowed by the state-of-the-art simulation techniques. Nevertheless, our results are in agreement with a variety of experimental data present in the literature, and allow us to formulate a molecular level model for the cAMP modulation of the HCN2 channel.

SUPPLEMENTARY MATERIAL

An online supplement to this article can be found by visiting BJ Online at http://www.biophysj.org.

We thank Prof. Vincent Torre and Marilisa Neri for useful discussions.

This work was financially supported by Ministero dell'Istruzione, dell'Universita' e della Ricerca (MURST-COFIN) and by Fondazione Cariparo.

REFERENCES

1. Mistrik, P., R. Mader, S. Michalakis, M. Weidinger, A. Pfeifer, and M. Biel. 2005. The murine HCN3 gene encodes a hyperpolarization-activated cation channel with slow kinetics and unique response to cyclic nucleotides. *J. Biol. Chem.* 280:27056–27061.
2. Yu, X., K. Duan, C. Shang, H. Yu, and Z. Zhou. 2004. Calcium influx through hyperpolarization-activated cation channels (I(h) channels) contributes to activity-evoked neuronal secretion. *Proc. Natl. Acad. Sci. USA.* 101:1051–1056.
3. Rosenbaum, T., and S. Gordon. 2004. Quickening the pace: looking into the heart of HCN channels. *Neuron.* 42:193–196.
4. Stieber, J., S. Herrmann, S. Feil, J. Loster, R. Feil, M. Biel, F. Hofmann, and A. Ludwig. 2003. The hyperpolarization-activated channel HCN4 is required for the generation of pacemaker action potentials in the embryonic heart. *Proc. Natl. Acad. Sci. USA.* 100: 15235–15240.
5. Robinson, R., and S. Siegelbaum. 2003. Hyperpolarization-activated cation currents: from molecules to physiological function. *Annu. Rev. Physiol.* 65:453–480.
6. Biel, M., A. Schneider, and C. Wahl. 2002. Cardiac HCN channels: structure, function, and modulation. *Trends Cardiovasc. Med.* 12:206–212.

7. Chen, J., D. Piper, and M. Sanguinetti. 2002. Voltage sensing and activation gating of HCN pacemaker channels. *Trends Cardiovasc. Med.* 12:42–45.
8. Accili, E., C. Proenza, M. Baruscotti, and D. DiFrancesco. 2002. From funny current to HCN channels: 20 years of excitation. *News Physiol. Sci.* 17:32–37.
9. Jan, L., and Y. Jan. 1990. A superfamily of ion channels. *Nature.* 345:672.
10. DiFrancesco, D., and P. Tortora. 1991. Direct activation of cardiac pacemaker channels by intracellular cyclic AMP. *Nature.* 351:145–147.
11. Ludwig, A., X. Zong, M. Jeglitsch, F. Hofmann, and M. Biel. 1998. A family of hyperpolarization-activated mammalian cation channels. *Nature.* 393:587–591.
12. Santoro, B., and G. Tibbs. 1999. The HCN gene family: molecular basis of the hyperpolarization-activated pacemaker channels. *Ann. N. Y. Acad. Sci.* 868:741–764.
13. Seifert, R., A. Scholten, R. Gauss, A. Mincheva, P. Lichter, and U. Kaupp. 1999. Molecular characterization of a slowly gating human hyperpolarization-activated channel predominantly expressed in thalamus, heart, and testis. *Proc. Natl. Acad. Sci. USA.* 96:9391–9396.
14. Ludwig, A., X. Zong, F. Hofmann, and M. Biel. 1999. Structure and function of cardiac pacemaker channels. *Cell. Physiol. Biochem.* 9:179–186.
15. Wainger, B., M. DeGennaro, B. Santoro, S. Siegelbaum, and G. Tibbs. 2001. Molecular mechanism of cAMP modulation of HCN pacemaker channels. *Nature.* 411:805–810.
16. Wang, J., S. Chen, and S. Siegelbaum. 2001. Regulation of hyperpolarization-activated HCN channel gating and cAMP modulation due to interactions of COOH terminus and core transmembrane regions. *J. Gen. Physiol.* 118:237–250.
17. Zagotta, W., N. Olivier, K. Black, E. Young, R. Olson, and E. Gouaux. 2003. Structural basis for modulation and agonist specificity of HCN pacemaker channels. *Nature.* 425:200–205.
18. Johnson, J. J., and W. Zagotta. 2005. The carboxyl-terminal region of cyclic nucleotide-modulated channels is a gating ring, not a permeation path. *Proc. Natl. Acad. Sci. USA.* 102:2742–2747.
19. Schultz, S., G. Shields, and T. Steitz. 1991. Crystal structure of a CAP-DNA complex: the DNA is bent by 90 degrees. *Science.* 253:1001–1007.
20. Clayton, G., W. Silverman, L. Heginbotham, and J. Morais-Cabral. 2004. Structural basis of ligand activation in a cyclic nucleotide regulated potassium channel. *Cell.* 119:615–627.
21. Taylor, S., J. Yang, J. Wu, N. Haste, E. Radzio-Andzelm, and G. Anand. 2004. PKA: a portrait of protein kinase dynamics. *Biochim. Biophys. Acta.* 1697:259–269.
22. Wu, J., S. Brown, N. Xuong, and S. Taylor. 2004. RI-α subunit of PKA: a cAMP-free structure reveals a hydrophobic capping mechanism for docking cAMP into site B. *Structure.* 12:1057–1065.
23. Rehmann, H., B. Prakash, E. Wolf, A. Rueppel, J. De Rooij, J. Bos, and A. Wittinghofer. 2003. Structure and regulation of the cAMP-binding domains of Epac2. *Nat. Struct. Biol.* 10:26–32.
24. Diller, T., N. Madhusudan Xuong, and S. Taylor. 2001. Molecular basis for regulatory subunit diversity in cAMP-dependent protein kinase: crystal structure of the type II beta regulatory subunit. *Structure.* 9:73–82.
25. Passner, J., S. Schultz, and T. Steitz. 2000. Modeling the cAMP-induced allosteric transition using the crystal structure of CAP-cAMP at 2.1 A resolution. *J. Mol. Biol.* 304:847–859.
26. Su, Y., W. Dostmann, F. Herberg, K. Durick, N. Xuong, L. T. Eyck, S. Taylor, and K. Varughese. 1995. Regulatory subunit of protein kinase A: structure of deletion mutant with cAMP binding domains. *Science.* 269:807–813.
27. Passner, J., and T. Steitz. 1997. The structure of a CAP-DNA complex having two cAMP molecules bound to each monomer. *Proc. Natl. Acad. Sci. USA.* 94:2843–2847.
28. Berman, H., L. Ten Eyck, D. Goodsell, N. Haste, A. Kornev, and S. Taylor. 2005. The cAMP binding domain: an ancient signaling module. *Proc. Natl. Acad. Sci. USA.* 102:45–50.
29. Capener, C., H. Kim, Y. Arinaminpathy, and M. Sansom. 2002. Ion channels: structural bioinformatics and modelling. *Hum. Mol. Genet.* 11:2425–2433.
30. Haider, S., A. Grottesi, B. Hall, F. Ashcroft, and M. Sansom. 2005. Conformational dynamics of the ligand-binding domain of inward rectifier K channels as revealed by molecular dynamics simulations: toward an understanding of Kir channel gating. *Biophys. J.* 88:3310–3320.
31. Law, R., R. Henchman, and J. McCammon. 2005. A gating mechanism proposed from a simulation of a human α7 nicotinic acetylcholine receptor. *Proc. Natl. Acad. Sci. USA.* 102:6813–6818.
32. Henchman, R., H. Wang, S. Sine, P. Taylor, and J. McCammon. 2005. Ligand-induced conformational change in the α7 nicotinic receptor ligand binding domain. *Biophys. J.* 88:2564–2576.
33. Giorgetti, A., and P. Carloni. 2003. Molecular modeling of ion channels: structural predictions. *Curr. Opin. Chem. Biol.* 7:150–156.
34. Pantano, S., M. Zaccolo, and P. Carloni. 2005. Molecular basis of the allosteric mechanism of cAMP in the regulatory PKA subunit. *FEBS Lett.* 579:2679–2685.
35. Matulef, K., G. Flynn, and W. Zagotta. 1999. Molecular rearrangements in the ligand-binding domain of cyclic nucleotide-gated channels. *Neuron.* 24:443–452.
36. Berman, H., J. Westbrook, Z. Feng, G. Gilliland, T. Bhat, H. Weissig, I. Shindyalov, and P. Bourne. 2000. The Protein Data Bank. *Nucleic Acids Res.* 28:235–242.
37. Ponder, J., and D. Case. 2003. Force fields for protein simulations. *Adv. Protein Chem.* 66:27–85.
38. Reference deleted in proof.
39. Wang, J., P. Cieplak, and P. Kollman. 2000. How well does a restrained electrostatic potential (RESP) model perform in calculating conformational energies of organic and biological molecules? *J. Comput. Chem.* 21:1049–1074.
40. Jorgensen, W., J. Chandrasekhar, J. Madura, and M. Klein. 1983. Comparison of simple potential functions for simulating liquid water. *J. Chem. Phys.* 79:926–935.
41. Punta, M., A. Cavalli, V. Torre, and P. Carloni. 2003. Molecular modeling studies on CNG channel from bovine retinal rod: a structural model of the cyclic nucleotide-binding domain. *Proteins.* 52:332–338.
42. Sagui, C., and T. Darden. 1999. Molecular dynamics simulations of biomolecules: long-range electrostatic effects. *Annu. Rev. Biophys. Biomol. Struct.* 28:155–179.
43. Essmann, U., L. Perera, M. Berkowitz, T. Darden, H. Lee, and L. Pedersen. 1995. A smooth particle mesh Ewald method. *J. Chem. Phys.* 103:8577–8593.
44. Darden, T., D. York, and L. Pedersen. 1993. Particle mesh Ewald: an *N*log(*N*) method for Ewald sums in large systems. *J. Chem. Phys.* 98: 10089–10092.
45. Hess, B., H. Bekker, H. Berendsen, and J. Fraaije. 1997. LINCS: a linear constraint solver for molecular simulations. *J. Comput. Chem.* 18:1463–1472.
46. Lindahl, E., B. Hess, and D. van der Spoel. 2001. GROMACS 3.0: a package for molecular simulation and trajectory analysis. *J. Mol. Model.* 7:306–317.
47. Berendsen, H. J. C., D. van der Spoel, and R. van Drunen. 1995. GROMACS: a message-passing parallel molecular dynamics implementation. *Comput. Phys. Comm.* 91:43–56.
48. Berendsen, H., J. Postma, A. DiNola, and J. Haak. 1984. Molecular dynamics with coupling to an external bath. *J. Chem. Phys.* 81:3684–3690.
49. Nosé, S. 1984. A molecular dynamics method for simulations in the canonical ensemble. *Mol. Phys.* 52:255–268.
50. Hoover, W. 1985. Canonical dynamics: equilibrium phase-space distributions. *Phys. Rev. A.* 31:1695–1697.
51. Nosé, S., and M. Klein. 1983. Constant pressure molecular dynamics for molecular systems. *Mol. Phys.* 50:1055–1076.
52. Parrinello, M., and A. Rahman. 1981. Polymorphic transitions in single crystals: a new molecular dynamics approach. *J. Appl. Phys.* 52:7182–7190.

53. Kazmierkiewicz, R., C. Czaplewski, B. Lammek, and J. Ciarkowski. 1999. Essential dynamics/factor analysis for the interpretation of molecular dynamics trajectories. *J. Comput. Aided Mol. Des.* 13:21–33.

54. Amadei, A., A. Linssen, and H. Berendsen. 1993. Essential dynamics of proteins. *Proteins.* 17:412–425.

55. Garcia, A. 1992. Large-amplitude nonlinear motions in proteins. *Phys. Rev. Lett.* 68:2696–2699.

56. Ichiye, T., and M. Karplus. 1991. Collective motions in proteins: a covariance analysis of atomic fluctuations in molecular dynamics and normal mode simulations. *Proteins.* 11:205–217.

57. Horiuchi, T., and N. Go. 1991. Projection of Monte Carlo and molecular dynamics trajectories onto the normal mode axes: human lysozyme. *Proteins.* 10:106–116.

58. Hess, B. 2002. Convergence of sampling in protein simulations. *Phys. Rev. E.* 65:031910.

59. Hess, B. 2000. Similarities between principal components of protein dynamics and random diffusion. *Phys. Rev. E.* 62:8438–8448.

60. Eisenhaber, F., P. Lijnzaad, P. Argos, C. Sander, and M. Scharf. 1995. The double cube lattice method: efficient approaches to numerical integration of surface area and volume and to dot surface contouring of molecular assemblies. *J. Comput. Chem.* 16:273–284.

61. Lee, B., and F. Richards. 1971. The interpretation of protein structures: estimation of static accessibility. *J. Mol. Biol.* 55:379–400.

62. Kabsch, W., and C. Sander. 1983. Dictionary of protein secondary structure: pattern recognition of hydrogen-bonded and geometrical features. *Biopolymers.* 22:2577–2637.

63. Micheletti, C., P. Carloni, and A. Maritan. 2004. Accurate and efficient description of protein vibrational dynamics: comparing molecular dynamics and Gaussian models. *Proteins.* 55:635–645.

64. Raschke, T., J. Tsai, and M. Levitt. 2001. Quantification of the hydrophobic interaction by simulations of the aggregation of small hydrophobic solutes in water. *Proc. Natl. Acad. Sci. USA.* 98:5965–5969.

65. Allen, T., O. Andersen, and B. Roux. 2004. On the importance of atomic fluctuations, protein flexibility, and solvent in ion permeation. *J. Gen. Physiol.* 124:679–690.

66. Karplus, M., and G. Petsko. 1990. Molecular dynamics simulations in biology. *Nature.* 347:631–639.

67. Zong, X., C. Eckert, H. Yuan, C. Wahl-Schott, H. Abicht, L. Fang, R. Li, P. Mistrik, A. Gerstner, B. Much, L. Baumann, S. Michalakis, R. Zeng, Z. Chen, and M. Biel. 2005. A novel mechanism of modulation of hyperpolarization-activated cyclic nucleotide-gated channels by Src kinase. *J. Biol. Chem.* 280:34224–34232.

68. Craven, K., and W. Zagotta. 2004. Salt bridges and gating in the COOH-terminal region of HCN2 and CNGA1 channels. *J. Gen. Physiol.* 124:663–677.